

## Rotational bands and noncollective structures in $^{85}\text{Zr}$

S. K. Tandel,\* S. R. Kore, and S. B. Patel

*Department of Physics, University of Mumbai, Vidyanageri, Mumbai-400 098, India*

S. Muralithar, R. P. Singh, and R. K. Bhowmik

*Nuclear Science Centre, P.O. Box 10502, New Delhi-110 067, India*

(Received 8 October 2001; published 23 April 2002)

The structure of the transitional nucleus  $^{85}\text{Zr}$  has been investigated through spectroscopy and lifetime measurements. States up to spins of  $\frac{45}{2}\hbar$  and  $\frac{39}{2}\hbar$  in the positive and negative parity bands, respectively, have been established through  $\gamma$ - $\gamma$  coincidence measurements. The results indicate that there is a competition between collective and noncollective modes of excitation. Two pronounced band crossings have been observed in the positive parity sequence, while none is evident in the negative parity states. The pattern of shape evolution in the positive and negative parity bands is markedly different. The results of the experiments qualitatively corroborate the predictions of total Routhian surface calculations.

DOI: 10.1103/PhysRevC.65.054307

PACS number(s): 23.20.Lv, 21.10.Ky, 21.10.Tg, 21.10.Re

### I. INTRODUCTION

The shape of nuclei with valence particles in the  $f$ - $p$ - $g$  shell is influenced by large gaps between the single-particle levels at various nucleon numbers for prolate and oblate deformations, as well as the spherical shell gap at nucleon number 50. These differing, and occasionally opposing influences, lead to the coexistence of different shapes and a rapid evolution in shape with a change in excitation energy and angular momentum. Nuclei with  $N \approx 45$  lie in the region of transition from deformed to spherical shapes, where these effects are particularly evident [1–5]. The structure of nuclei in the Zr isotopic chain [6,7] is seen to vary from strongly collective through moderately deformed to near spherical, with an increase in neutron number toward  $N=50$ . The nucleus  $^{85}\text{Zr}$  ( $N=45$ ) is therefore particularly suitable for studying these phenomena. Although the neighboring odd  $A$  isotones viz.  $^{81}\text{Kr}$ ,  $^{83}\text{Sr}$ , and  $^{87}\text{Mo}$  [8–10] have been studied in detail, information about high-spin states in  $^{85}\text{Zr}$  was lacking. Therefore, two experiments were performed, the first to determine the level structure of the excited states. In the second experiment the lifetimes of the levels in the rotational bands were sought to be determined using the DSAM technique.

### II. EXPERIMENTAL PROCEDURE AND LINE-SHAPE ANALYSIS

Excited states in the nucleus  $^{85}\text{Zr}$  were populated using  $^{31}\text{P}$  and  $^{32}\text{S}$  beams obtained from the 15 UD pelletron at Nuclear Science Center, New Delhi, India. These beams were made incident on enriched  $^{58}\text{Ni}$  and natural Fe foils during the course of two experiments to determine the level structure and lifetimes of states in  $^{85}\text{Zr}$ . The  $^{58}\text{Ni}(^{31}\text{P}, 3pn)^{85}\text{Zr}$  reaction, using a 130-MeV  $^{31}\text{P}$  beam, was utilized to determine the structure of excited states through  $\gamma$ - $\gamma$  coincidence measurements. The  $^{58}\text{Ni}$  target had a thick-

ness of  $550 \mu\text{g}/\text{cm}^2$  and was enriched to  $>99\%$  purity. Twelve high-purity, Compton-suppressed Ge detectors from the Gamma Detector Array (GDA) were used to record  $\gamma$ - $\gamma$  coincidence data. There were four detectors each at  $49^\circ$ ,  $98^\circ$ , and  $144^\circ$  with respect to the beam direction. The  $\gamma$  multiplicity information was recorded by a 14 element BGO filter. In the second experiment, to determine the  $E2$  transition strengths, the reaction  $^{56}\text{Fe}(^{32}\text{S}, 2pn)^{85}\text{Zr}$ , with a 120-MeV  $^{32}\text{S}$  beam, was used. The target was a thick ( $\approx 20 \text{ mg}/\text{cm}^2$ ) natural Fe foil. During this experiment, there were only six detectors in the GDA, two each at the forward and backward angles and another two at  $98^\circ$ . The  $\gamma$ - $\gamma$  coincidence data were acquired using the program FREEDOM running on a Linux platform. The data were collected and sorted offline into  $4k \times 4k$  matrices, and one-dimensional energy spectra were extracted from these matrices by gating on the appropriate energies. The analysis of the spectroscopic data was carried out using the programs FREEDOM and RADWARE.

The analysis of the data from the lifetime experiment was performed in the following manner. The velocity distributions were calculated using a Monte Carlo simulation program with the shell-corrected Northcliffe and Schilling stopping powers [11]. These velocity histories were converted into time-dependent velocity profiles for both the forward and backward angle detectors. The theoretical line shapes were generated by the program LINESHAPE [12], and the lifetimes were obtained by minimizing  $\chi^2$  obtained from a comparison of these with the experimental line shapes. The details regarding the line-shape analysis can be found elsewhere [13].

### III. RESULTS

The level structure of  $^{85}\text{Zr}$  was studied previously [14] up to an excitation energy of 6.2 MeV in the positive parity band and 4.8 MeV in the negative parity band. It has been possible to determine states up to an excitation energy of 11.1 MeV and a spin of  $\frac{45}{2}\hbar$  in the positive parity band, and up to 9.2 MeV and  $\frac{39}{2}\hbar$  in the negative parity band. Evidence

\*Email address: sujit@nuclear.mu.ac.in

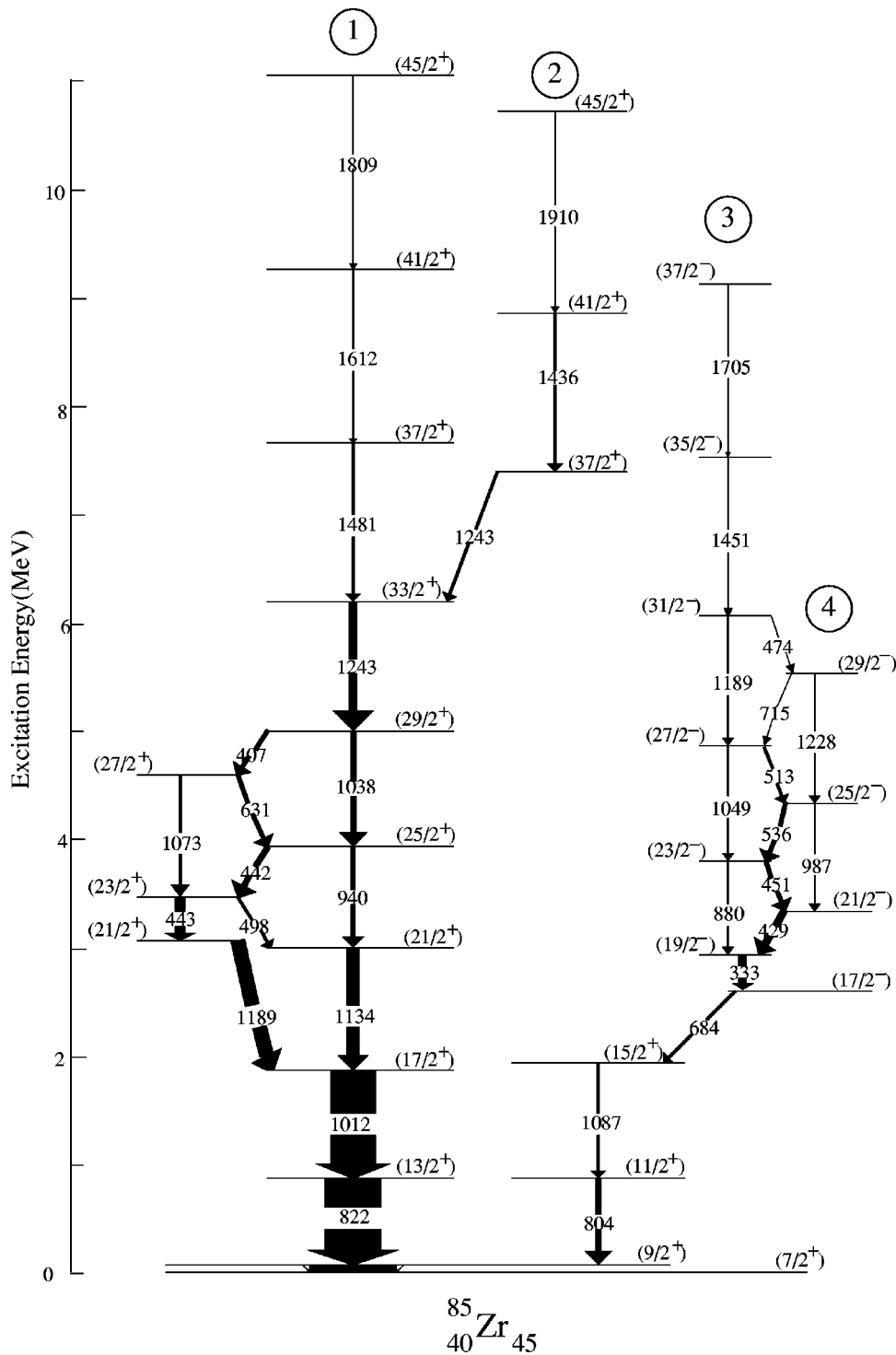


FIG. 1. Partial level scheme for  $^{85}\text{Zr}$ .

of a second band crossing has been observed in the positive parity states, while none is visible in the negative parity states. Since no low-energy  $\gamma$  detectors were used in the present work, and as the threshold for the Ge detectors was set to be around 80 keV, coincidences between the 50-keV transition deexciting the  $\frac{9}{2}^+$  state and the other  $\gamma$  rays in  $^{85}\text{Zr}$  could not be observed. The level scheme at low spins, determined from this work, is in good agreement with the one obtained from the previous work [14]. However, for reasons of clarity and in order to highlight the high-spin data ob-

tained, only one of the several decay branches constituting the deexcitation of the low-spin single particle states, has been shown in Fig. 1. The multiplicities for the observed transitions are based on those obtained from the previous work, and, for in-band  $\gamma$  rays at high spin, an electric quadrupole character has been assumed.

There is a forking in intensity observed above the  $\frac{33}{2}^+$  state in the positive parity sequence (band 1 in Fig. 1) and two distinct branches (bands 1 and 2), having comparable intensities, are observed upto a spin of  $\frac{45}{2}\hbar$ . Band 2 lies

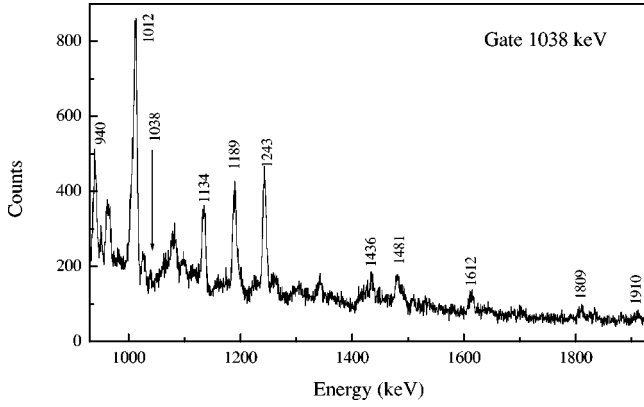


FIG. 2. Transitions in the positive parity band of  $^{85}\text{Zr}$ , as seen in the gate on the 1038-keV  $\gamma$  ray.

lower in energy than band 1, above the  $\frac{33}{2}^+$  state. The  $\gamma$  rays constituting bands 1 and 2 have been shown in the gated spectrum for the 1038-keV transition in Fig. 2 and the 1243-keV transition in Fig. 3. In the negative parity sequence, band 3 is favored and is observed up to high spins. The other branch (band 4) becomes unfavored and is not seen beyond a spin of  $\frac{29}{2}\hbar$ . The energies and relative intensities of the  $\gamma$ -ray transitions shown in Fig. 1 are listed in Table I.

Lifetimes for only three levels in the positive parity band could be determined. Due to the lack of statistics in the DSAM data, it was possible to use only the spectra obtained by gating on the transitions below the  $\gamma$  rays of interest, for the line-shape analysis. The transitions deexciting the  $\frac{13}{2}^+$  and the  $\frac{17}{2}^+$  states appear to be fully stopped in the DSAM data, indicating lifetimes which are much longer than the stopping times of the evaporation residues in the target. The 1134-, 940-, and 1038-keV  $\gamma$  rays have discernible line shapes, as does the 1243-keV transition. The experimental and fitted line shapes for the 1134-keV transition are shown in Fig. 4. However, the 1243-keV line being a doublet and all the  $\gamma$  rays below having a coincidence with both components of the doublet, it was not possible to extract the lifetimes of

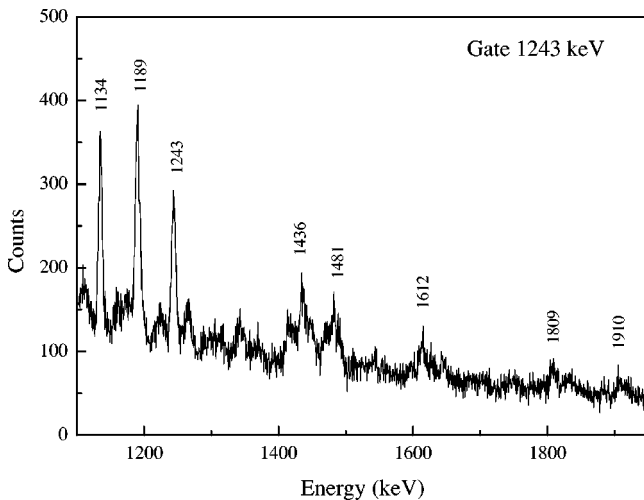


FIG. 3. Transitions in the positive parity band of  $^{85}\text{Zr}$ , as seen in the gate on the 1243-keV  $\gamma$  ray.

TABLE I. Initial level and  $\gamma$ -ray energies, spins of initial and final states, and relative intensities for the transitions in  $^{85}\text{Zr}$ . The uncertainty in the energies of the transitions is about 1 keV for a 1-MeV transition.

$E_{lev}$ (keV)	$E_\gamma$ (keV)*	$I_i^\pi(\hbar)$	$I_f^\pi(\hbar)$	$I_\gamma$ (rel)
Positive parity band				
854	804	(11/2 <sup>+</sup> )	(9/2 <sup>+</sup> )	12.5(2)
872	822	(13/2 <sup>+</sup> )	(9/2 <sup>+</sup> )	100
1884	1012	(17/2 <sup>+</sup> )	(13/2 <sup>+</sup> )	79.7(5)
1941	1087	(15/2 <sup>+</sup> )	(11/2 <sup>+</sup> )	9.1(2)
2625	684	(17/2 <sup>-</sup> )	(15/2 <sup>+</sup> )	8.8(2)
3018	1134	(21/2 <sup>+</sup> )	(17/2 <sup>+</sup> )	24.6(3)
3073	1189	(21/2 <sup>+</sup> )	(17/2 <sup>+</sup> )	29.1(4)
3516	498	(23/2 <sup>+</sup> )	(21/2 <sup>+</sup> )	8.5(2)
3516	443	(23/2 <sup>+</sup> )	(21/2 <sup>+</sup> )	20.7(3)
3958	940	(25/2 <sup>+</sup> )	(21/2 <sup>+</sup> )	10.1(2)
3958	442	(25/2 <sup>+</sup> )	(23/2 <sup>+</sup> )	12.9(2)
4589	1073	(27/2 <sup>+</sup> )	(23/2 <sup>+</sup> )	6.9(2)
4589	631	(27/2 <sup>+</sup> )	(25/2 <sup>+</sup> )	10.9(3)
4996	1038	(29/2 <sup>+</sup> )	(25/2 <sup>+</sup> )	12.2(2)
4996	407	(29/2 <sup>+</sup> )	(27/2 <sup>+</sup> )	10.0(2)
6239	1243	(33/2 <sup>+</sup> )	(29/2 <sup>+</sup> )	17.2(3)
7482	1243	(37/2 <sup>+</sup> )	(33/2 <sup>+</sup> )	9.2(3)
7720	1481	(37/2 <sup>+</sup> )	(33/2 <sup>+</sup> )	7.3(2)
8918	1436	(41/2 <sup>+</sup> )	(37/2 <sup>+</sup> )	7.8(2)
9332	1612	(41/2 <sup>+</sup> )	(37/2 <sup>+</sup> )	6.3(2)
10828	1910	(45/2 <sup>+</sup> )	(41/2 <sup>+</sup> )	4.5(3)
11141	1809	(45/2 <sup>+</sup> )	(41/2 <sup>+</sup> )	4.3(3)
Negative parity band				
2958	333	(19/2 <sup>-</sup> )	(17/2 <sup>-</sup> )	17.3(2)
3387	429	(21/2 <sup>-</sup> )	(19/2 <sup>-</sup> )	14.6(2)
3838	880	(23/2 <sup>-</sup> )	(19/2 <sup>-</sup> )	2.5(1)
3838	451	(23/2 <sup>-</sup> )	(21/2 <sup>-</sup> )	9.2(1)
4374	987	(25/2 <sup>-</sup> )	(21/2 <sup>-</sup> )	5.2(2)
4374	536	(25/2 <sup>-</sup> )	(23/2 <sup>-</sup> )	9.1(2)
4887	1049	(27/2 <sup>-</sup> )	(23/2 <sup>-</sup> )	4.0(1)
4887	513	(27/2 <sup>-</sup> )	(25/2 <sup>-</sup> )	7.3(1)
5602	1228	(29/2 <sup>-</sup> )	(25/2 <sup>-</sup> )	3.9(3)
5602	715	(29/2 <sup>-</sup> )	(27/2 <sup>-</sup> )	2.9(2)
6076	1189	(31/2 <sup>-</sup> )	(27/2 <sup>-</sup> )	5.1(1)
6076	474	(31/2 <sup>-</sup> )	(29/2 <sup>-</sup> )	1.2(1)
7527	1451	(35/2 <sup>-</sup> )	(31/2 <sup>-</sup> )	6.5(2)
9232	1705	(39/2 <sup>-</sup> )	(35/2 <sup>-</sup> )	3.1(3)

either the  $\frac{33}{2}^+$  or  $\frac{37}{2}^+$  levels. Further, it was observed that the  $E2$  transitions in the negative parity band for which sufficient statistics could be obtained in the gated spectra appear to be almost completely stopped. Therefore, it was not feasible to reliably extract lifetimes, and as a result, the line-shape analysis was not performed for the negative parity band.

#### IV. DISCUSSION

The structure of the odd  $A$  isotones  $^{81}\text{Kr}$  ( $Z=36$ ),  $^{83}\text{Sr}$  ( $Z=38$ ), and  $^{87}\text{Mo}$  ( $Z=42$ ) has been experimentally deter-

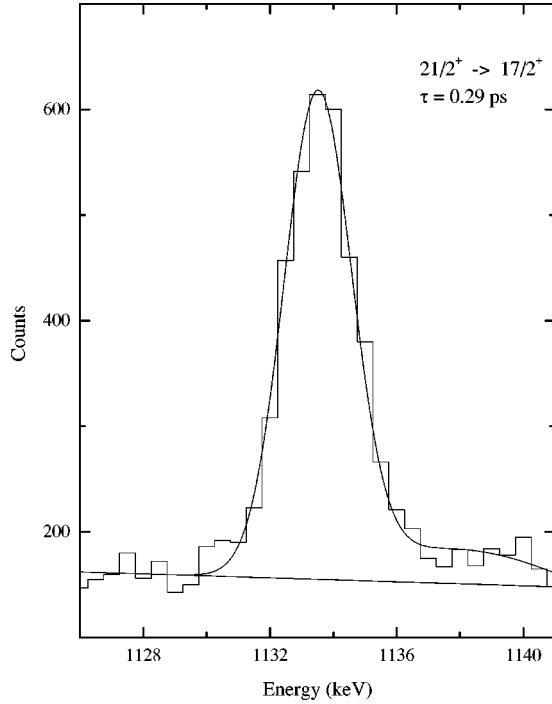


FIG. 4. Experimental data and line-shape fit for the 1134-keV transition in the positive parity band.

mined up to large values of spin [8–10]. It has been found that the proton number plays a major role in influencing the shape, especially after the first proton alignment in the positive parity band. The negative parity bands, which result from the occupation of the  $f_{5/2}$ ,  $p_{3/2}$ , and  $p_{1/2}$  orbitals by the valence particles, in addition to the  $g_{9/2}$  subshell, exhibit a behavior distinct from the positive parity states. These and other aspects of the structure of  $^{85}\text{Zr}$  ( $Z=40$ ) were sought to be determined in the present work.

### Positive parity states

The positive parity levels at low excitation can be grouped into two distinct categories viz. the collective states which are part of the rotational band and those arising from single-particle excitations. A large number of these single-particle levels are present at low spin [14]. The level structure for  $^{85}\text{Zr}$ , shown in Fig. 1, shows only one of the single-particle branches (the 1087- and 684-keV transitions). The signature splitting between the favored and unfavored branches in the one-quasiparticle positive parity rotational band is large, indicative of a decoupled configuration. In this band, there is a forking of intensity above the  $\frac{17}{2}^+$  state into two branches. A pronounced band crossing, with a very weak band interaction, is visible above the  $\frac{21}{2}^+$  state at a frequency  $\hbar\omega=0.52$  MeV (Fig. 5). This results from the breaking of a  $g_{9/2}$  proton pair, since the neutron crossing is blocked. The decrease in collectivity, immediately following the first crossing, is evident from the values of the transition quadrupole moments ( $Q_t$ ), extracted from the DSAM measurement (Table II). The  $M1$  transition rates above the  $\frac{21}{2}^+$  state increase considerably. This is associated with a corresponding decrease in the signature splitting. At higher excitation, away

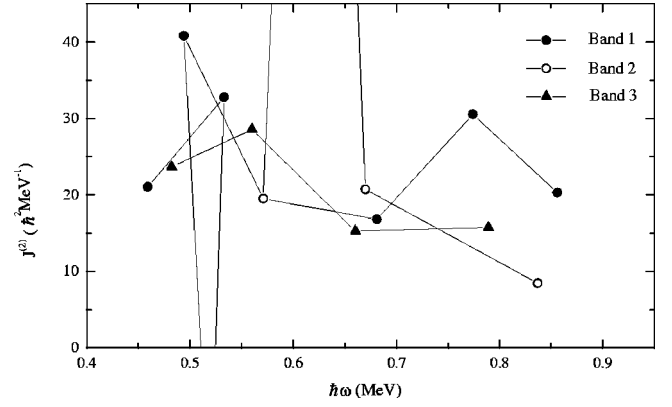


FIG. 5. Dynamic moments of inertia  $J^{(2)}$  for the positive and negative parity bands in  $^{85}\text{Zr}$ .

from the first band crossing, the gain in collectivity is apparent from the deduced  $Q_t$  values. The signature splitting again increases and only the favored branch (band 1) is seen above a spin  $\frac{29}{2}\hbar$ .

Another forking in intensity is visible above the  $\frac{33}{2}^+$  state. A pronounced crossing is seen in one of the branches (Fig. 5), while no alignment is evident in the other branch (band 1). The branch in which the alignment is observed is the five-quasiparticle branch (band 2). It becomes yrast and carries the major fraction of the intensity. The gain in alignment is much more gradual in the collective branch (Fig. 6). Both the branches, the five-quasiparticle band and the collective branch, are seen to continue up to a spin of  $\frac{45}{2}\hbar$ . The dynamic moment of inertia  $J^{(2)}$  for the five-quasiparticle branch decreases sharply to much below the rigid body value ( $\approx 23\hbar^2$  MeV $^{-1}$ ) as the  $\frac{45}{2}^+$  state is approached, while it remains in the vicinity of the rigid body value for the collective branch (Fig. 5). This indicates the large contribution to the total angular momentum from the aligned quasiparticles in the five-quasiparticle branch. The second alignment at  $\hbar\omega=0.62$  MeV, is a  $BC$  neutron crossing, since the proton  $BC$  crossing is blocked by the aligned pair from the first ( $AB$ ) proton crossing. These crossing frequencies are very similar to those in the positive parity band of  $^{84}\text{Zr}$ , where the first alignment occurs at  $\hbar\omega=0.48$  MeV and the second one at  $\hbar\omega=0.59$  MeV. The proton or neutron character of the crossings is also the same in both nuclei.

### Negative parity states

The negative parity levels in  $^{85}\text{Zr}$  result mainly from the occupation of the  $p_{1/2}$  orbital by the unpaired neutron. These

TABLE II. Lifetimes, transition strengths, and quadrupole moments of a few states in the positive parity band of  $^{85}\text{Zr}$ .

$E_\gamma$ (keV)	$I_i^\pi \rightarrow I_f^\pi$ ( $\hbar$ )	$\tau$ (ps)	$B(E2)$ (W.u.)	$ Q_t $ (eb)
1134	$(21/2^+) \rightarrow (17/2^+)$	$0.29^{(0.03)}_{(0.04)}$	$89^{(5)}_{(6)}$	$2.61^{(0.15)}_{(0.19)}$
940	$(25/2^+) \rightarrow (21/2^+)$	$1.16^{(0.37)}_{(0.40)}$	$58^{(9)}_{(10)}$	$2.01^{(0.32)}_{(0.35)}$
1038	$(29/2^+) \rightarrow (25/2^+)$	$0.42^{(0.04)}_{(0.04)}$	$97^{(5)}_{(5)}$	$2.51^{(0.13)}_{(0.13)}$

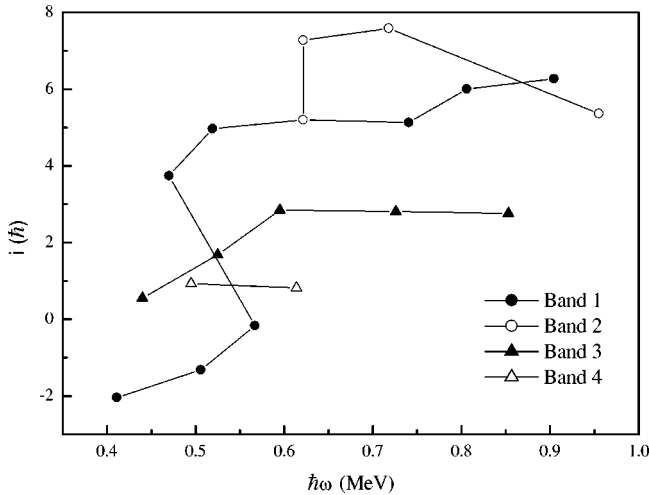


FIG. 6. Quasiparticle alignments for the positive and negative parity bands in  $^{85}\text{Zr}$ . A reference rotor with  $J_0 = 18 \text{ MeV}^{-1}\hbar^2$  and  $J_1 = 0$  was used in the calculations.

states are nonyrast compared to the positive parity levels, and are therefore weakly populated. The negative parity rotational band is a strongly coupled one, compared to the positive parity band, which is apparent from the strong  $M1$  transitions observed. This behavior is similar to the other  $N = 45$  isotones [8–10]. The  $E2$  transitions in the negative parity band, for which sufficient statistics could be obtained, are almost completely stopped in the DSAM data. Further, there are no pronounced band crossings visible, unlike the positive parity band. These factors seem to indicate that the magnitude of deformation for the negative parity band is quite different from the positive parity states. The gain in alignment in the negative parity band (band 3) is very gradual, and is about  $3\hbar$  over a frequency range of approximately  $0.2 \text{ MeV}$  (Fig. 6). Beyond a frequency of  $0.6 \text{ MeV}$ , the magnitude of alignment does not change. The signature splitting in the negative parity band is small up to a spin  $\frac{29}{2}\hbar$ , beyond which the magnitude of splitting increases suddenly (Fig. 7). The unfavored signature branch (band 4) is not observed above this point.

### Predicted shape evolution

The shapes of the positive and negative parity bands in  $^{85}\text{Zr}$  were determined by performing Hartree-Fock-Bogolyubov cranking calculations, using a Woods-Saxon potential and a short-range monopole pairing force [15]. The BCS pairing formalism was used and the Strutinsky shell correction procedure was employed. The total Routhian surfaces (TRS's) were calculated in a  $(\beta_2, \gamma)$  mesh for various rotational frequencies and, at each mesh point, the total energy was minimized with respect to the hexadecapole deformation  $\beta_4$ . The results of the TRS calculations can be summarized as follows.

For the favored signature in the positive parity band, at a rotational frequency  $\hbar\omega = 0.4 \text{ MeV}$  [Fig. 8(a)], shallow energy minima are seen in two distinct regions in the  $(\beta_2, \gamma)$  plane. The minimum at  $(\beta_2, \gamma) = (0.23, -53^\circ)$  corresponds to an almost oblate shape, with moderate deformation. The

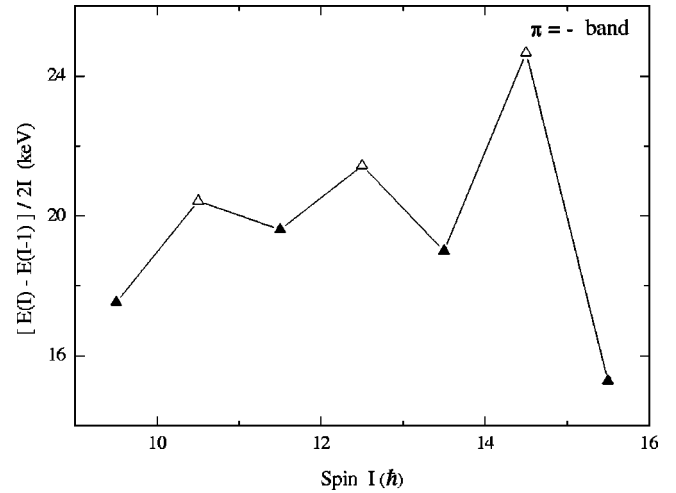


FIG. 7. Signature splitting in the negative parity band of  $^{85}\text{Zr}$ .

second energy minimum is seen for a spherical shape. These features exhibit good agreement with the level schemes obtained from the present work and from previous work [14], wherein rotational and single-particle structures are found to coexist up to  $3 \text{ MeV}$  of excitation. At  $\hbar\omega = 0.9 \text{ MeV}$  [Fig. 8(b)], a well-defined minimum is seen at  $(\beta_2, \gamma) = (0.05, +4^\circ)$ , reflecting the loss in collectivity at high spin. In addition, a secondary minimum at  $(\beta_2, \gamma) = (0.24, -55^\circ)$  is obtained, which is slightly higher in energy (around  $500 \text{ keV}$ ) than the first minimum. This aspect is mirrored in the experimental level structure, wherein the five-quasiparticle band becomes yrast after the second band crossing, while the continuation of the collective branch lies about  $300\text{--}400 \text{ keV}$  higher in terms of excitation energy. The loss in collectivity in the five-quasiparticle branch is also visible from the  $J^{(2)}$  moment of inertia obtained from the experimental level structure, which is seen to drop sharply below the rigid body value. On the other hand, the secondary energy minimum, for a moderate oblate deformation, corresponds to the continuation of the collective band, which lies higher in energy compared to the five-quasiparticle band. It is possible to extract the transition quadrupole moment  $(Q_t)$  predicted by the TRS calculations using the relations

$$(Q_t)_{\gamma=0^\circ} = 0.0109ZA^{2/3}\beta_2(1 + 0.36\beta_2),$$

$$(Q_t)_{\gamma \neq 0^\circ} = (Q_t)_{\gamma=0^\circ} \frac{\cos(\gamma + 30^\circ)}{\cos(30^\circ)}.$$

For a rotational frequency  $\hbar\omega = 0.4 \text{ MeV}$  in the positive parity band, a value of  $2.26 \text{ eb}$  is predicted by the TRS calculations, which compares reasonably well with the values  $2.61$  and  $2.51 \text{ eb}$  obtained below and above the first band crossing, from the DSAM measurement.

For both the signatures of negative parity band, a rather smaller oblate deformation  $(\beta_2, \gamma) = (0.12, -60^\circ)$  is predicted by the calculations. Figure 8(c) shows the TRS for the favored signature at a rotational frequency  $\hbar\omega = 0.4 \text{ MeV}$ . The predicted low value of the quadrupole deformation is

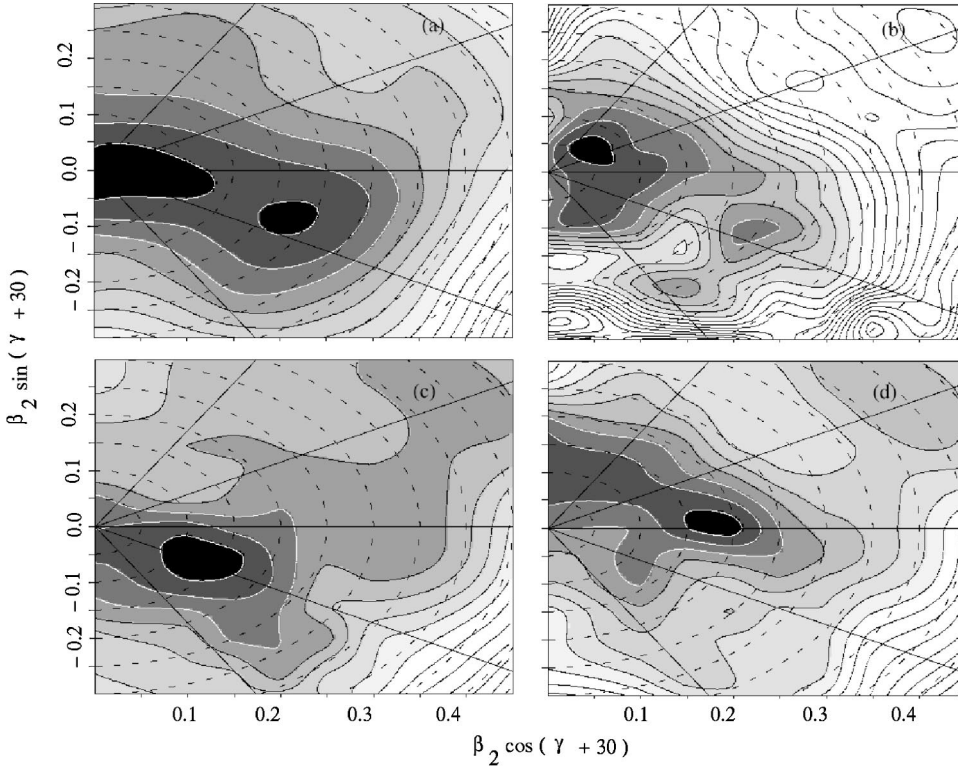


FIG. 8. Total Routhian surfaces for the favored signatures in the positive and negative parity bands of  $^{85}\text{Zr}$ . The darker regions are lower in energy than the lighter ones. (a) and (b) The  $\pi = +$  band at  $\hbar\omega = 0.4$  and  $0.9$  MeV, respectively. (c) and (d) The  $\pi = -$  band at  $\hbar\omega = 0.4$  and  $0.5$  MeV, respectively.

supported by the weak in-band  $E2$  transitions observed and also by the fact that these  $\gamma$  rays did not exhibit discernible lineshapes, indicating either long half-lives or feeding times. At a frequency  $\hbar\omega = 0.5$  MeV, the minimum in energy is obtained for a triaxial shape [Fig. 8(d)], at  $(\beta_2, \gamma) = (0.18, -28^\circ)$ . This change to a triaxial shape is associated with an increase in the magnitude of signature splitting in the experimental level structure. The shape transition is probably responsible for the absence of an alignment in the negative parity states, in contrast to the positive parity states, where pronounced crossings are seen at  $\hbar\omega = 0.52$  and  $0.62$  MeV.

#### Systematics for the $N = 45$ isotones

A comparison of the positive and negative parity bands in the odd  $A$ ,  $N = 45$  isotones  $^{81}\text{Kr}$ ,  $^{83}\text{Sr}$ ,  $^{85}\text{Zr}$ , and  $^{87}\text{Mo}$  [8–10] leads to the following observations. The positive parity states in these nuclei, below the first proton crossing, are similar. The bandhead is the  $\frac{7}{2}^+$  state, with a small (few tens of keV) energy separation between the  $\frac{7}{2}^+$  and the  $\frac{9}{2}^+$  states. Enhanced  $E2$  transitions are observed between the  $\frac{13}{2}^+$  and the  $\frac{9}{2}^+$  and the  $\frac{17}{2}^+$  and the  $\frac{13}{2}^+$  states, indicative of a rotational behavior. The transition strengths in this region of spin are larger in the case of Kr ( $Z = 36$ ) as compared to Mo ( $Z = 42$ ). This situation is reversed above the  $\frac{21}{2}^+$  state. Two states with a spin  $\frac{21}{2}\hbar$  are observed in the positive parity bands of all the isotones. The states which are built upon the  $\frac{21}{2}^+$  level, which is lower in excitation energy, constitute the three-quasiparticle band. The other states built upon the  $\frac{21}{2}^+$  level, which is higher in excitation energy, constitute the one-quasiparticle band. The following features are evident: (i) The magnitude of the deformation in the isotones is found to vary with spin. The trend of this variation is different for

$^{81}\text{Kr}$ , where it is found to decrease substantially above the  $\frac{21}{2}^+$  level, while there is a marked increase in the case of  $^{87}\text{Mo}$ , with the Sr and Zr isotones exhibiting an intermediate behavior. (ii) The relative population of the one- and three-quasiparticle bands follows a different pattern. The three-quasiparticle band is not observed above the  $\frac{21}{2}^+$  level in  $^{81}\text{Kr}$ , while the same is true for the one-quasiparticle band in  $^{87}\text{Mo}$ . These observations, taken together, indicate that the magnitude of deformation in these nuclei is strongly dependent on the number of protons in the nucleus. This is due to the fact that with an increase in the number of protons above the shell gap for oblate deformation, expected at  $Z = 36$ , the collective behavior becomes more pronounced. The first band crossing in the heavier isotones is due to the alignment of a pair of  $g_{9/2}$  protons. Such a crossing is not observed in  $^{81}\text{Kr}$ , probably due to the lower magnitude of deformation. The negative parity bands in these isotones, which appear to have a similar and smaller magnitude of deformation as compared to the positive parity states in the heavier isotones, therefore exhibit a similar behavior.

#### V. SUMMARY

The high-spin structure of  $^{85}\text{Zr}$  has been investigated, and the evolution of shape in both the positive and negative parity states has been studied. The measured transition strengths and the calculated total Routhian surfaces indicate a moderate oblate deformation for the positive parity band. At low spins, this is found to coexist with an almost spherical shape. At the highest spins, a considerable loss in collectivity is evident. The magnitude of the deformation in the negative

parity band is significantly less compared to the positive parity band. A change in shape from oblate to triaxial occurs at a rotational frequency of  $\hbar\omega \approx 0.5$  MeV in the negative parity band. The difference in shapes probably leads to the markedly different behavior of the positive and negative parity bands, with both proton and neutron  $g_{9/2}$  alignments being seen in the positive parity states and none being observed in the negative parity band. In order to obtain a better understanding of some of the above mentioned aspects, it is essential to study the lifetimes of some of the longer lived states through the recoil distance technique. Further, a DSAM measurement with sufficient statistics, to determine the level

lifetimes and feeding times at the highest spins, is also necessary.

#### ACKNOWLEDGMENTS

The authors would like to gratefully acknowledge the support provided by the pelletron staff at Nuclear Science Centre during both the runs required for this work. S.K.T. would like to thank John Wells for providing the LINESHAPE program and subsequent helpful discussions. Funding from the Board of Research in Nuclear Sciences, India, and the University of Mumbai, India, for a part of this work, is also appreciated.

- 
- [1] K. Jonsson, B. Cederwall, A. Johnson, R. Wyss, T. Back, J. Cederkall, M. Devlin, J. Elson, D. R. LaFosse, F. Lerma, D. G. Sarantites, R. M. Clark, I. Y. Lee, A. O. Machiavelli, and R. W. Macleod, *Nucl. Phys.* **A645**, 47 (1999).
  - [2] S. L. Tabor, J. Doring, G. D. Johns, R. A. Kaye, G. N. Sylvan, C. J. Gross, Y. A. Akovali, C. Baktash, D. W. Stracener, P. F. Hua, M. Korolija, D. R. LaFosse, D. G. Sarantites, F. E. Durham, I. Y. Lee, A. O. Machiavelli, W. Rathbun, and A. Vander Molen, *Phys. Rev. C* **56**, 142 (1997).
  - [3] J. Doring, R. Schwengner, L. Funke, H. Rotter, G. Winter, B. Cederwall, F. Liden, A. Johnson, A. Atac, J. Nyberg, and G. Sletten, *Phys. Rev. C* **50**, 1845 (1994).
  - [4] S. L. Tabor, P. D. Cottle, C. J. Gross, U. J. Hüttmeier, E. F. Moore, and W. Nazarewicz, *Phys. Rev. C* **39**, 1359 (1989).
  - [5] E. F. Moore, P. D. Cottle, C. J. Gross, D. M. Headly, U. J. Huttmeier, S. L. Tabor, and W. Nazarewicz, *Phys. Rev. C* **38**, 696 (1988).
  - [6] U. J. Huttmeier, C. J. Gross, D. M. Headly, E. F. Moore, S. L. Tabor, T. M. Cormier, P. M. Stwertka, and W. Nazarewicz, *Phys. Rev. C* **37**, 118 (1988).
  - [7] T. D. Johnson, A. Aprahamian, C. J. Lister, D. J. Blumenthal, B. Crowell, P. Chowdhury, P. Fallon, and A. O. Machiavelli, *Phys. Rev. C* **55**, 1108 (1997).
  - [8] L. Funke, J. Doring, P. Kemnitz, E. Will, G. Winter, A. Johnson, L. Hildingsson, and Th. Lindblad, *Nucl. Phys.* **A455**, 206 (1986).
  - [9] C. Baktash, D. M. Cullen, J. D. Garrett, C. J. Gross, N. R. Johnson, W. Nazarewicz, D. G. Sarantites, J. Simpson, and T. R. Werner, *Phys. Rev. Lett.* **74**, 1946 (1995).
  - [10] Ch. Winter, D. J. Blumenthal, P. Chowdhury, B. Crowell, P. J. Ennis, S. J. Freeman, C. J. Lister, C. J. Gross, J. Heese, A. Jungclaus, K. P. Lieb, D. Rudolph, M. A. Bentley, W. Gelletly, J. Simpson, J. L. Durell, and B. J. Varley, *Nucl. Phys.* **A535**, 137 (1991).
  - [11] L. C. Northcliffe and R. F. Schilling, *Nucl. Data Tables* **7**, 233 (1970).
  - [12] J. C. Wells (private communication).
  - [13] S. K. Tandel, S. B. Patel, M. Gupta, S. Muralithar, R. P. Singh, and R. K. Bhowmik (unpublished).
  - [14] A. Jungclaus, S. Albers, P. von Brentano, M. Eschenauer, A. Harder, K. P. Lieb, M. Luig, N. Nicolay, D. Rudolph, and M. Weiszflog, *Z. Phys. A* **352**, 3 (1995).
  - [15] W. Nazarewicz, J. Dudek, R. Bengtsson, T. Bengtsson, and I. Ragnarsson, *Nucl. Phys.* **A435**, 397 (1985).